VLEO Satellite Constellation Design for Regional Aviation and Marine Coverage

Guoquan Chen, *Graduate Student Member, IEEE*, Shaohua Wu, *Member, IEEE*, Yajing Deng, Jian Jiao, *Member, IEEE*, Qinyu Zhang, *Senior Member, IEEE*

***Abstract*—Recently, the Space-Air-Ground-Sea Integrated Network (SAGSIN) attracts great attention due to its ability to provide high-speed communication services to aviation users (AUs) and marine users (MUs), with Low Earth Orbit (LEO) satellites play an essential role. However, available LEO space is nearly saturated and full of massive space junks, which, combined with the ultra-low latency requirements for future 6G, presents a significant challenge. To address this issue, we propose designing a Very Low Earth Orbit (VLEO)-based satellite network that efficiently serves AUs and MUs. We first create heat maps based on the actual collected data and generate a benchmark observation point model with grid point method. Then we propose an implicit multi-objective continuous multivariate optimization problem to achieve the maximum coverage with minimum VLEO satellites. To solve this problem, we build a constellation simulation system, using the idea of decomposition and polymerization combined with the elite strategic genetic algorithm (ESGA) of swarm intelligence optimization algorithm. Many simulation results are obtained, including the indication that the optimal VLEO constellation has the deployment features of large altitude and low inclination, and has better coverage performance for longitudinal distributed business. The constellation design process is also highly migratory for other non-terrestrial networks.**

***Index Terms*—SAGSIN, VLEO, satellite constellation, swarm intelligence optimization algorithm, ESGA.**

I. Introduction

ALTHOUGH the improving 5G network has powerful communication capabilities that provide high-speed, high-capacity, low-latency and reliable communication services to terrestrial mobile users [1], it is still challenging to meet the demands of aviation users (AUs) and marine users (MUs) for high speed and stable communication services. Initially, Geosynchronous Earth Orbit (GEO) satellite communication system was the primary system for AUs [2] and MUs [3]. However, due to the limitation of orbital altitude, GEO satellites inherently have a significant disadvantage of high latency, and have gradually lost the researchers' interest. With the continuous improvement of 5G communication technology, the Space-Air-Ground-Sea Integrated Network (SAGSIN) [4]–[6] architecture has gained research attention, and researchers have started making clear plans for the scenarios and goals of 6G communication. Based on this and given the fact that both aviation traffic and marine traffic are growing rapidly year by year [7]–[11], heterogeneous hybrid satellite communication networks have been developed in order to solve the access problems of AUs and MUs [12], and the research results related to resource allocation have become more [13]. Among them, Low Earth Orbit (LEO) satellites play an essential role due to their ability to achieve global coverage with low transmission delay and more flexible network access services [14], [15], and the research on LEO satellites based on the SAGSIN context has become more plentiful [16], [17].

Compared to the GEO satellite, which orbits at an altitude of 35,786km, the LEO satellite's altitude range is generally between 500-2000km. Although the cost of networking and maintenance for LEO satellite constellations is relatively high and there will be more frequent handovers during communication, its single-hop delay can be controlled within 30ms, making it highly suitable for personal communication services. Therefore, in research and construction related to heterogeneous hybrid satellite networks [18], LEO satellites have demonstrated superior performance in terms of low latency and high-speed communication service requirements [19], [20]. LEO broadband satellite network systems, featuring low orbit and a large scale, are showing a worldwide booming trend [21]. In recent years, low-earth orbit has become the focus of global space development, and countries are paying more attention to satellite development, especially LEO satellites. Competition for orbital resources is becoming increasingly intense, and the mass deployment of LEO satellite constellations is entering a peak period. Meanwhile, the accelerated process of the LEO giant constellations [22] has set off a new trend of communication research associated with it [23]–[26].

Constructing LEO satellite networks involves several stages, and the constellation design is considered to be the first and most important stage since it directly impacts the overall system performance [27], [28]. In addition, thanks to the on-board solar panel power system, satellites are able to change orbit and thus realize the dynamic adjustment of the constellation network, therefore continuous rapid constellation design is also pursued in the current field of space communication, in particular for hotspot area communications and emergency communications under the condition of limited constellation resources. Several classical and basic constellations, such as the Walker Delta [29], the Walker Star [30], and the Flower satellite constellation [31], [32], were proposed at an early stage. Based on them, Mortari *et al.* [33] considered the concept of ultra-dense LEO satellite constellation to balance

This work has been supported in part by the National Key Research and Development Program of China under Grant no. 2020YFB1806403, and in part by the Guangdong Basic and Applied Basic Research Foundation under Grant no. 2022B1515120002. *(Corresponding author: Shaohua Wu.)*

G. Chen and Y. Deng are with the Department of Electronics and Information Engineering, Harbin Institute of Technology (Shenzhen), Shenzhen 518055, China (email: 180210217@stu.hit.edu.cn; hitdengyj@163.com).

S. Wu, J. Jiao and Q. Zhang are with the Guangdong Provincial Key Laboratory of Aerospace Communication and Networking Technology, Harbin Institute of Technology (Shenzhen), Shenzhen 518055, China, and also with the Peng Cheng Laboratory, Shenzhen 518055, China (e-mail: hitwush@hit.edu.cn; jiaojian@hit.edu.cn; zqy@hit.edu.cn).

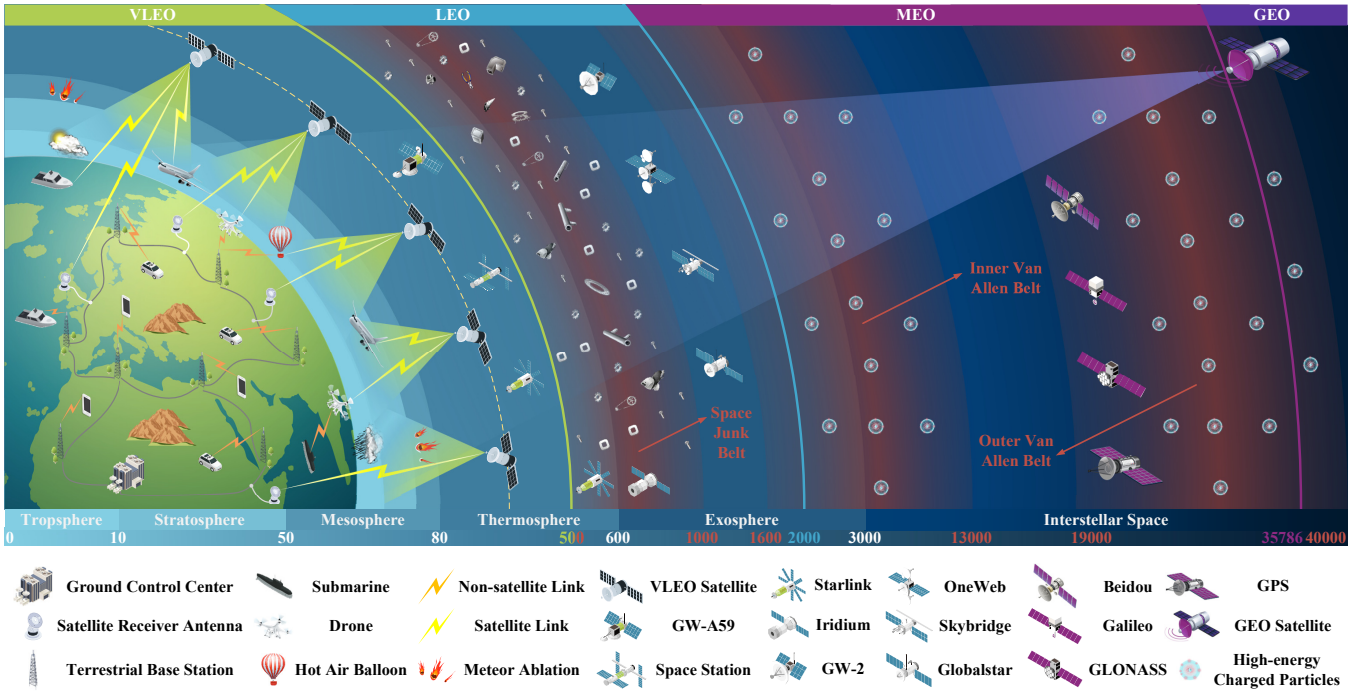

Fig. 1. SAGSIN architecture with VLEO satellite constellation. (GNSS in the MEO layer and geosynchronous satellite system in the GEO layer are considered)

network performance and deployment cost. In addition, in terms of coverage metrics consideration in satellite constellation design, to optimize the multi-area coverage performance of satellite systems with high robustness and reliability, Chen *et al.* [34] proposed a LEO microsatellite formation design method based on the Flower constellation design theory. Wang *et al.* [35] proposed a multi-layer LEO satellite constellation deployment scheme that takes into account the mobility of satellites and can support seamless coverage on a global scale.

However, achieving seamless global coverage may not be practical for developing countries where LEO satellite constellation development is still in its initial stages. Therefore, it is more practical to establish a satellite constellation that can achieve ideal coverage for AUs and MUs in the target region. Although a model of coastal distributed antennas for providing data transmission services to the marine internet of things was proposed by authors in [36], the communication distance of coastal distributed antennas is far from sufficient for most vessels at sea, especially far offshore, not to mention AUs in the air. Moreover, including those mentioned above, most of the papers' LEO constellation design works are based on a virtual traffic model and do not focus on the obtainment and analysis of real data. Although this would cost more finance, time and effort, the real traffic distribution is more practical and instructive[1]. Considering the fact that LEO orbital space is nearly saturated and has massive space junks [37] (as shown in Fig. 1), and given the many advantages of Very Low Earth Orbit (VLEO) satellites themselves, such as higher revisiting frequency, higher optical resolution, lower payload costs, lower risk of space debris collision, and lower levels of cosmic particle radiation [37], the United States, Russia, China, and several European countries have started to resume the construction of VLEO satellite constellations. Therefore, there is an urgent demand for research on the design of VLEO constellations. It will be of high reference and guidance value to design VLEO satellite constellations for regional aviation communication traffic (ACT) and marine communication traffic (MCT) based on fresh business data.

In this work, we aim to design an optimal-coverage VLEO constellation with minimum satellites. The following aspects should be taken into consideration. *Firstly*, acquisition of real data will be emphasized to ensure the practicability of our model. *Secondly*, constellation simulation system deployment and modern optimization algorithms must be considered to address the unique and complex challenges associated with constellation design optimization problems. The specific contributions of our work can be summarized as follows.

- We focus on the Automatic Dependent Surveillance Broadcast (ADS-B) system and Automatic Identification System (AIS) of Chinese aviation and coastal regions to ensure the authenticity and freshness of the data. Then we analyze and generate the corresponding heat maps of ACT and MCT, and use the grid point method to establish the benckmark observation point (BOP) model respectively.
- We derive the average coverage expression. In the context of VLEO constellation design, we propose an implicit[2] multi-objective continuous multivariate (IMOCM) optimization problem of minimizing the satellite scale and maximizing the average coverage. In the constellation model we consider

[1]In this article, the real communication traffic data work for aviation and costal region in China would be considered and added with emphasis.

[2]The objective function is generally divided into explicit and implicit, the latter indicates that there is no specific expression for the objective function, but the objective function value still exists.

the more diverse Walker constellation model, where most possibilities of Walker Delta and Walker Star are included.

• We adopt the "divide and conquer" methodology and propose a constellation-based "three-stage" solution. We combine the swarm intelligence optimization algorithm and the satellite constellation simulation analysis method, the latter involves the construction of a constellation system. The simulation results indicate that the optimal constellation has the deployment features of large altitude, low inclination and is oriented to longitudinal distribution business. These results have a certain reference and guidance value for the less studied VLEO constellation.

• The solution in this work is highly migratory, and a rapid constellation design considering genetic algorithm makes it possible for continuous constellation design pursuing real-time performance, especially for hotspot area communication scenarios and emergency communication scenarios under the condition of limited constellation resources. It also provide some new insights for the non-terrestrial network design, such as unmanned aerial vehicle (UAV) networks, airship platform networks, *etc*.

The rest of this article is organized as follows. In Section II, we introduce the considered system model. The derivation of relevant formulas and analytical modeling of the problem are given in Section III. In Section IV, we propose a "three-stage" solution for the optimization problem. Simulation results are given in Section V, followed by conclusions in Section VI.

II. System Model

In this section, as shown in Fig. 1[3], we first describe the SAGSIN architecture based on VLEO satellites, where those AUs and MUs who can not access the terrestrial network can only obtain communication services through VLEO satellites. Combined with the fact of the extremely short transit time of the VLEO satellite, more satellites need to be placed to obtain more satisfactory coverage. We assume that all satellites are divided into P planes in altitude h, denoted by $\mathcal{P} = \{1, 2, ..., P\}$, and orbit plane $p \in \mathcal{P}$ consist of N_p VLEO satellites, denoted by $\mathcal{N}_p = \{1, 2, ..., N_p\}$. Then $n_p \in \mathcal{N}_p$ denotes a specific satellite in orbital plane p and the total number of satellites can be calculated by

$$N_{\text{tot}} = \sum_{p=1}^{P} N_p. \tag{1}$$

A. The Primary Business Distribution Model

The main characteristics of the users are mainly reflected in the distribution of their business needs. In the context of the future SAGSIN architecture of 6G, in addition to the traditional ground users, the VLEO satellite communication system mostly serves two other types of services, *i.e.*, users

[3]The numbers in the figure indicate the altitude in *km*. The Van Allen radiation belt contains charged high-energy particles that can cause some harm to satellites, but GNSS is generally at about 20,000 km, which is the edge of the outer Van Allen belt, so the impact is not significant. And the parameters related to astronomy, if not otherwise specified, refer to the NASA official website, which will not be repeated hereafter.

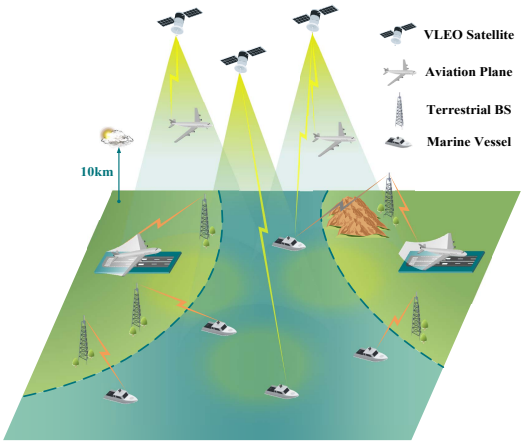

Fig. 2. VLEO satellite role and communication scenario schematic.

on board aircraft navigating at high altitude and users on board vessels sailing on the marine surface. For both types of users, as shown in Fig. 2, terrestrial networks can only serve them at specific times, such as during the takeoff and landing phases of an aircraft and when a vessel is close to shore. For most of the time, terrestrial communications are out of reach, and satellite communication systems can make a big difference.

1) ADS-B: As shown in Fig. 2, when the aircraft is not during the takeoff and landing phases but in the stratosphere (about 10 km), the VLEO satellites provide the main communication service for the aircraft since it is not able to access the ground communication network. By collecting, parsing and filtering the ADS-B information sources, we can obtain the Chinese traffic distribution status of aviation communication business. Symbol $\mathcal{A} = \{1, 2, ..., A\}$ is the set of all aircrafts, and the maximum passenger capacity and passenger load factor of aircraft $a \in \mathcal{A}$ is located by $c_a^{\max}$ and l_a, while $\overline{l_a}$ is the average value of all aircrafts.

For convenience, we divide the entire surface of the Earth into 180×360 grids at 1° interval of longitude and latitude, denoted by the set $\mathcal{G} = \{1, 2, ..., G\}$. And we assume that the business traffic per AU is a constant value $\overline{T_a^u}$. Then the business traffic of aircraft a can be expressed as

$$T_a = c_a^{\max} \cdot \overline{l_a} \cdot \overline{T_a^u}, \forall a \in \mathcal{A}, \tag{2}$$

and the aviation business traffic of grid g can be given by

$$T_g^{\text{air}} = \sum_{a \in g} T_a, \forall g \in \mathcal{G}. \tag{3}$$

Let $\overline{l_a} = 0.7$ and $\overline{T_a^u} = 0.5$Mbps [38], combined with the processed ADS-B system snapshot data, we can obtain the final ACT heat map of the target area which is shown in Fig. 3(a,c). It depicts that the ACT in China is mainly concentrated in the southeastern coastal region and the corresponding airspace over the adjacent sea area. The Yangtze River Delta region and the Pearl River Delta region are two hotspots.

2) AIS: Considering that MCT are mostly gathered in offshore areas, we focus on the communication business in the southeast coastal area of China. As shown in Fig. 2, VLEO satellites provide the primary communication service

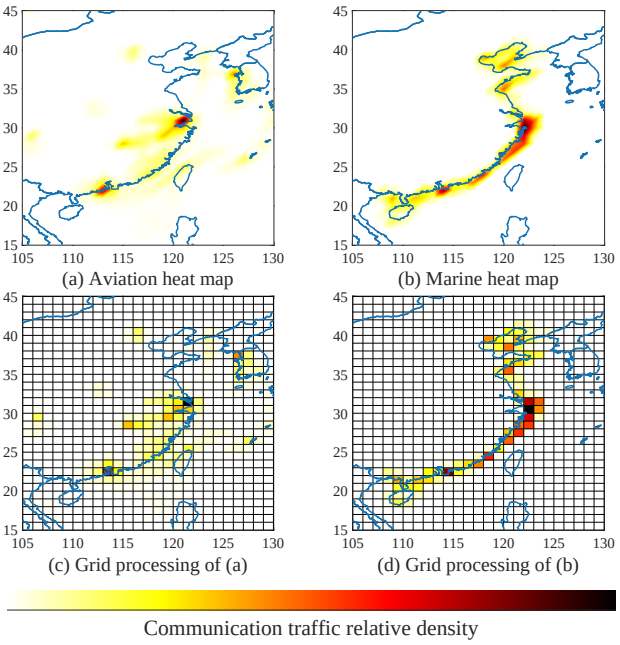

Fig. 3. Communicaiton traffic heat map of aviation and marine of target area.

for vessels when they are not docked, as they do not have access to the terrestrial communication network. By decoding AIS packets, the distribution of marine communication service traffic can be obtained. Symbol $\mathcal{V} = \{1, 2, ..., V\}$ is the set of all vessels, and the maximum passenger capacity and passenger load factor of vessel $v \in \mathcal{V}$ are denoted by $c_v^{\max}$and l_v, while $\overline{l_v}$ is the average value of all vessels.

We assume that the business traffic per MU is a constant value $\overline{T_v^u}$. Then the business traffic of vessel v can be expressed as

$$T_v = c_v^{\max} \cdot \overline{l_v} \cdot \overline{T_v^u}, \forall v \in \mathcal{V}, \tag{4}$$

and the marine business traffic of grid g can be given by

$$T_g^{\text{marine}} = \sum_{v \in g} T_v, \forall g \in \mathcal{G}, \tag{5}$$

then based on the 10 days monitoring data in the southeast coastal region of China, we can obtain the final MCT heat map which is shown in Fig. 3(b,d). It depicts that the MCT in China is largely uniformly distributed along the southeastern coastal region, with the Yangtze River Delta region and the Pearl River Delta region are also two hotspots for MCT.

B. VLEO Satellite Orbital Elements and Constellation Model

For the design of LEO satellite constellations, the Walker Delta (Rosette) and the Walker Star (90° inclination) are two common and popular approaches [39], where their orbital planes obey the 360° and 180° homogeneity rules, respectively. The Walker constellation all have circular orbits and is commonly described as $(N_W/P_W/F_W)$, where N_W, P_W, and F_W denote the total number of satellites, the number of satellite planes, and the phase factor, respectively. The phase factor F_W, which is a integer between 0 and $(P_W - 1)$, can be used to determine the phase difference Δu between the corresponding satellites in two adjacent orbital planes as follows:

$$\Delta u = \frac{360}{N_W} \cdot F_W, F_W \in [0, P_W - 1], F_W \in \mathbb{Z}^+, \tag{6}$$

and we have $P \in \{P_W\}$ VLEO satellite planes and the number of satellites of each plane can be expressed as

$$N_P = N_p = \frac{N_{\text{tot}}}{P}, \forall p \in \mathcal{P}. \tag{7}$$

Given the circular orbit, whose eccentricity e and perigee angle w are 0, then the other four orbital elements are:

1) Semi-major axis a_s: In the case of circular orbits, it is equal to the radius of the orbit r_s, *i.e.*, $a_s = r_s$.

2) Inclination i: Angle measured counterclockwise from the ecliptic to the planet's orbital plane at the ascending node. In this article, we consider i is range in [0°, 90°][4] when we design VLEO satellite constellation.

3) Longitude of right ascending node Ω: The tensor angle formed by measuring counterclockwise from the vernal equinox to the ascending node, when viewed over the North Pole, in the range [0°, 360°].

4) Mean Anomaly M_A: This is a hypothetical quantity describing the angle swept by the satellite in its auxiliary circular orbit as it starts to move with an average angular velocity from perigee. Assuming that the average angular velocity of the satellite moving in orbit is $\overline{w_v}$ and the moment at perigee is t_0, then M_A can be calculated as follows:

$$M_A = \overline{w_v} \cdot (t - t_0), \tag{8}$$

where t denotes the current moment.

Among all the orbital elements, only the true anomaly τ_A, the mean anomaly M_A, and the eccentric anomaly E_A change vary with different measurement times t_0, which determine the specific position of the satellite in orbit. The angular range of these three symbols is [0°, 360°] and the relationship between the three symbols τ_A, M_A and E_A is shown as follows:

$$\cos\tau_A = \frac{\cos E_A - e}{1 - e \cdot \cos E_A}, \tag{9}$$

$$M_A = E_A - e \cdot \sin E_A, \tag{10}$$

therefore, the position of each satellite in Cartesian coordinate can be calculated by

$$\begin{pmatrix} x \\ y \\ z \end{pmatrix} = (h + R_e) \begin{bmatrix} \cos\Omega\cos(w + \tau_A) - \sin\Omega\sin(w + \tau_A)\cos i \\ \sin\Omega\cos(w + \tau_A) + \cos\Omega\sin(w + \tau_A)\cos i \\ \sin i \cdot \sin(w + \tau_A) \end{bmatrix} \tag{11}$$

where R_e denotes the mean radius of the Earth[5]. Fig. 4 can help to interpret the physical meaning of some parameters.

In this article, for a more comprehensive study of the VLEO constellation design, we consider a more diverse Walker constellation, *i.e.*, the Ω-interval of the neighboring order planes

[4]Retrograde orbit satellite, *i.e.*, $i \in [90^o, 180^o]$, will not be considered due to the demand for a significant proportion of the orbiting energy to counteract the Earth's rotation.

[5]The equatorial radius of the Earth is about 6378.14 km, the polar radius is about 6356.75 km, and the mean radius is about 6371 km. Due to the limitation of the simulation software the value used in this article is 6378.19 km, *i.e.*, R_e = 6378.19 km.

are continuous (instead of the homogeneous rule) and the phase differences are continuized rather than discretized. For convenience, meanwhile we respectively take the former and the latter as Ω and M_A of the seed satellite (1^{st} satellite in 1^{st} plane), and denote them by Ω^{seed} and M_A^{seed}.

C. VLEO Satellite Other Related Parameters

1) VLEO Satellite Orbital Period T_s & Orbital Altitude h: The orbit of VLEO satellites is typically designed as a reentry orbit, and its period T_s satisfies the following equation:

$$\frac{T_s}{T_e} = \frac{z_1}{z_2}, z_j \in \mathbb{Z}^+, j = 1, 2, \tag{12}$$

where T_e is the period of the Earth's rotation[6]. According to the Kepler's Third Law, *i.e.*,

$$a_s^3 = K(T_s)^2, \tag{13}$$

where K is the Kepler constant[7] and since we have $r_s = R_e + h$, orbital altitude h can then be expressed as

$$h = \sqrt[3]{K(T_e \cdot \frac{z_1}{z_2})^2} - R_e, z_j \in \mathbb{Z}^+, j = 1, 2, \tag{14}$$

where upper and lower bounds on h are considered as follows:

• $h_{\max}$: Since we consider the VLEO satellite constellation, we set $h_{\max}$ to 500km according to [37].

• $h_{\min}$: Taking into account the restrictions on national airspace[8], atmospheric conditions[9], the Van Allen radiation belt, and the magnetic storm incident of Starlink in 2022[10], we set $h_{\min}$ to 250km.

2) VLEO Satellite Sensor Tension Angle β: The definition of the satellite sensor tension angle β is shown in Fig. 4 and it is directly determined by R_e, h, and the minimum elevation angle $\theta_{\min}$, as expressed by the following equation:

$$\beta = 2 \cdot \arcsin(\frac{R_e}{h + R_e} \cdot \cos\theta_{\min}). \tag{15}$$

Without loss of generality, $\theta_{\min}$ is generally taken as 10°.

3) VLEO Satellite Constellation Minimum Number $N_{\text{tot}}^{\min}$: According to Fig. 4, the coverage area of a satellite can be calculated by

$$S_s = 2\pi R_e^2(1 - \cos\frac{\phi}{2}). \tag{16}$$

Therefore the theoretical minimum value of the satellite size to achieve full coverage is

$$N_{\text{tot}}^{\min} = S_t / S_s, \tag{17}$$

where S_t is the area of the target area and $N_{\text{tot}}^{\min}$ is actually a rough minimum because of the area overlap phenomenon in circular coverage.

[6]The exact value of *23*h *56*m *4*s is used for the discussion and subsequent experimental simulations in this article, *i.e.*, $T_e = 86164$s instead of 24 hours.

[7]In this article, we take the value of $398601.98\text{km}^3/\text{s}^2$.

[8]Internationally, the airspace within 100km is generally classified as national airspace, which cannot be entered without permission.

[9]Thermospheric gases have huge impact on highly mobile VLEO satellites.

[10]More than 40 satellites of the Starlink system had crashed during the launch of the Earth's magnetic storms, based on which the United States set 250km as the minimum atmospheric safety altitude of satellites.

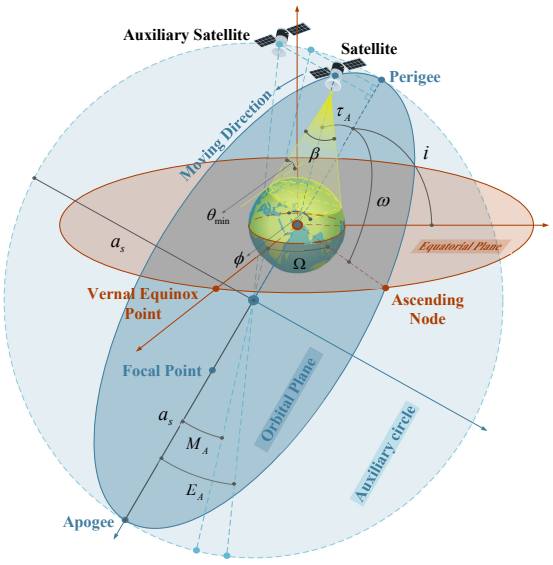

Fig. 4. Satellite six orbital elements and other related parameters.

III. Analysis and Problem Formulation

In this section, we first analyze the ACT distribution and the MCT distribution for the target area using the grid point method [40] and generate BOPs $o \in \mathcal{O}$ respectively, where $\mathcal{O} = \{1, 2, ..., O\}$. Then we use them to analyze and define the observation coverage C_o and the average coverage $\overline{C}$ of the target area to lay the foundation for the subsequent modeling of the optimization problem.

A. Target Area and BOP Analysis

Since the target area is a regional area and belongs to the low latitude region, as shown in Fig. 5 and Fig. 6, we can consider the grid point method to grid the traffic of the target area to be studied and generate the BOPs, the distribution of which can present and reflect the spatial distribution characteristics of the real ACT and MCT.

From Fig. 3(c) and Fig. 3(d), we can know that the longitudinal and latitudinal distribution ranges of them in the target area are [104°E-128°E, 22°N-40°N] and [108°E-124°E, 18°N-40°N]. We divide the total observation time T_{tot} into multiple time slots and use the binary variables $o_a(t)$ and $o_v(t)$ to denote whether the observation point o is covered or not by the satellite constellation at the time slot $t \in \mathcal{T} = \{1, 2, ..., T_{\text{tot}}\}$ under aviation and marine businesses, respectively. As show in the following equation:

$$o_{a/v}(t) = \begin{cases} 0, \text{beyond coverage}, \\ 1, \text{within coverage}. \end{cases} \quad t \in \mathcal{T}, \tag{18}$$

where a indicates aviation and v indicates marine.

What should be noted is that the subsequent analytical discussion and problem formulation will not distinguish between aviation and marine, *i.e.*, the corner scale settings of a and v will be ignored, because of the generality of the problem formulation.

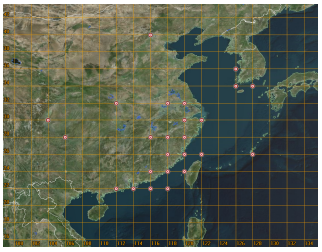

Fig. 5. ACT-BOP map.

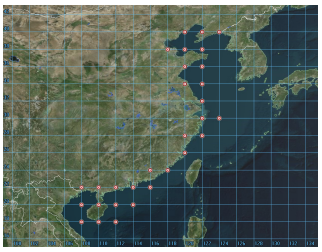

Fig. 6. MCT-BOP map.

Algorithm 1: ESGA to $\mathfrak{x}$

Input: P, N_P, $\mathcal{O}$, $\mathfrak{M}$, $\mathfrak{T}_{\text{gmax}}$, $\mathbf{I} = [h, i, \Omega, M_A]$, constraints in eq. (29).

Initialization: Random initial population $\mathfrak{P}_0$;
while *current generation* $\mathfrak{T}_g \leq \mathfrak{T}_{\text{gmax}}$ **do**
  for *each individual* $\mathbf{I}$ **do**
    Get the attributes $[h, i, \Omega, M_A]$ of $\mathbf{I}$;
    Build constellation in Satellite Software;
    for *each observation* o **do**
      Calculate C_o base on eq. (20);
    Calculate $\overline{C}$ based on eq. (21);
  Calculation of individual fitness $\mathfrak{F}(\mathbf{I})$;
  Fitness ranking, replicate top $\mathfrak{N}$ elite individual $\mathbf{I}_{\mathfrak{N}}$;
  Coding $\mathfrak{C}$; Selection Φ; Crossover Γ; Mutation Ψ;
  Decoding, obtain the next generation population $\mathfrak{P}$;
  $\mathfrak{T}_g = \mathfrak{T}_g + 1$;
Select the optimal individual;

Output: $\overline{C}_{\max}$, $\mathbf{I}_{\text{opt}} = [h_{\text{opt}}, i_{\text{opt}}, \Omega_{\text{opt}}^{\text{seed}}, M_{A_{\text{opt}}}^{\text{seed}}]$.

B. VLEO Satellite Constellation Coverage Analysis

Obviously $o(t)$ is a function of the parameters of the satellite constellation, set it be $F(\cdot)$, then $o(t)$ can be given by

$$o(t) = F(N_P, P, h, e, i, \Omega, \omega, M_A), \forall t \in \mathcal{T}. \tag{19}$$

Therefore, the observation coverage C_o can be given by

$$C_o = \frac{\sum_{t=1}^{T_{\text{tot}}} o(t)}{T_{\text{tot}}} = \frac{1}{T_{\text{tot}}} \sum_{t=1}^{T_{\text{tot}}} F(N_P, P, h, e, i, \Omega, \omega, M_A), \tag{20}$$

the average coverage of the target area $\overline{C}$, can thus be given as follows:

$$\overline{C} = \frac{1}{O} \sum_{o \in \mathcal{O}} C_o = \frac{1}{OT_{\text{tot}}} \sum_{o \in \mathcal{O}} \sum_{t=1}^{T_{\text{tot}}} F(N_P, P, h, e, i, \Omega, \omega, M_A), \tag{21}$$

where $N_{\text{tot}} = N_P \times P$ also necessarily as a function of the $\overline{C}$ and the parameters of the satellite constellation, set it be $F_r(\cdot)$, then N_{tot} can be calculated by

$$N_{\text{tot}} = F_r(\overline{C}, h, e, i, \Omega, \omega, M_A). \tag{22}$$

C. Problem Formulation

Considering the sustainability and the practical utilization of the system in operation, we set a low cost, high coverage rate satellite constellation as our ultimate goal.

1) Objective function: Low-cost, high-coverage satellite constellation construction is considered.

- Minimum total number of satellites

$$\min\ N_{\text{tot}} = F_r(\overline{C}, h, i, \Omega, M_A). \tag{23}$$

- Maximum average coverage rate (circular orbit)

$$\max \overline{C} = \frac{1}{O} \sum_{o \in \mathcal{O}} C_o = \frac{1}{OT_{\text{tot}}} \sum_{o \in \mathcal{O}} \sum_{t=1}^{T_{\text{tot}}} F(N_P, P, h, i, \Omega, M_A). \tag{24}$$

2) Constraints: Based on the relevant analysis in Section II, we can obtain the following constraints.

- Six orbital elements constraints

$$\begin{cases} 250 \leq h \leq 500, \\ 0^\circ \leq i \leq 60^\circ, \\ 0^\circ \leq \Omega, M_A \leq 360^\circ, \end{cases} \tag{25}$$

and we have $e, w = 0$.

- Reentry period constraint[11]

$$\begin{cases} h = \sqrt[3]{K(T_e \cdot \frac{z_1}{z_2})^2} - R_e, \\ z_j \in \mathbb{Z}^+, j = 1, 2. \end{cases} \tag{26}$$

- Satellite constellation number constraint

$$\begin{cases} N_{\text{tot}} = N_P \times P, N_{\text{tot}} \geq N_{\text{tot}}^{\min}, \\ N_P, P \in \mathbb{Z}^+. \end{cases} \tag{27}$$

Therefore, we can obtain the optimization problem $\mathfrak{X}$ as

$$\begin{aligned} (\mathfrak{X}): \min\ & N_{\text{tot}},\ -\overline{C}, && \text{(28a)} \\ \text{s.t.}\ & 250 \leq h \leq 500, && \text{(28b)} \\ & 0^\circ \leq i \leq 90^\circ, && \text{(28c)} \\ & 0^\circ \leq \Omega, M_A \leq 360^\circ, && \text{(28d)} \\ & h = \sqrt[3]{K(T_e \cdot \frac{z_1}{z_2})^2} - R_e, && \text{(28e)} \\ & N_{\text{tot}} = N_P \times P, N_{\text{tot}} \geq N_{\text{tot}}^{\min}, && \text{(28f)} \\ & z_j, N_P, P \in \mathbb{Z}^+, j = 1, 2. && \text{(28g)} \end{aligned}$$

The optimization problem $\mathfrak{X}$ can be found to be a complex IMOCM optimization problem. For the special characteristics of $\mathfrak{X}$, the traditional optimization algorithm can not help, we consider the use of modern optimization algorithms.

The expression of the objective function is implicit, and the function value needs to be obtained by building a satellite simulation system. Combining the fact that N_P and P belong to integers, this article considers to solve $\mathfrak{X}$ from the perspective of sub-cases with the combination of N_P and P.

[11]Since the value of z_1, z_2 can be artificially set, we can choose a proper value for them to guarantee that T_s satisfies eq. (12). Then this constraint can be ignore in the later simulation, *i.e.*, h can take any value in [250km, 500km].

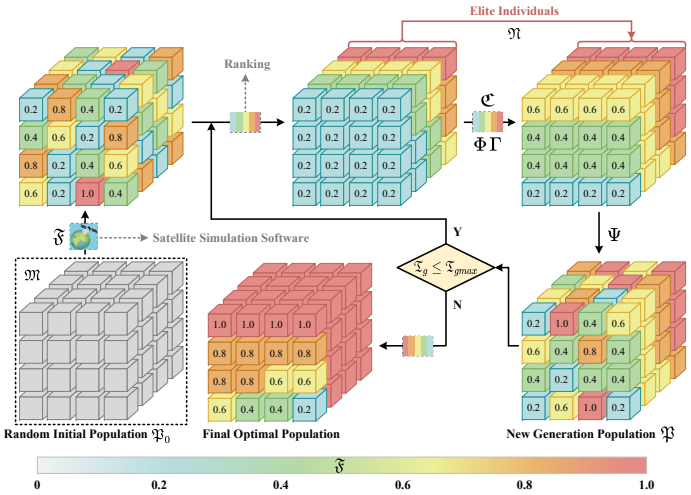

Fig. 7. The simplified flow illustration of ESGA.

IV. A Three-stage Solution Method

Considering that some intelligent algorithms have been well applied to the optimization of LEO satellite constellation design [41]–[43], this article considers the application of swarm intelligent optimization algorithms to solve $\mathfrak{X}$.

And in order to reduce the number of variables introduced during swarm intelligence optimization and to further improve the accuracy of the results, given the fact that N_P and P are discrete variables, we consider a "divide and conquer" methodology to solve $\mathfrak{X}$ from the perspective of N_{tot}. Briefly, we first consider the decomposition of $\mathfrak{X}$ into multiple single-objective optimization problems. Then, swarm intelligence optimization is performed for each of them. Finally, the results are combined to obtain the optimal solution of $\mathfrak{X}$.

A. Stage 1: Decomposition and Decoupling

Due to the complexity of $\mathfrak{X}$ and the interaction between the objective functions, we consider decomposing the optimization problem $\mathfrak{X}$ into N_{tot} single-objective optimization problems $\mathfrak{x}_k, k \in \{1,2,...,N_{\text{tot}}\}$ from the perspective of N_{tot} to achieve the decoupling effect of the objective functions. Then factorize k and represent the sub-optimization problem under the l^{th} constellation hierarchy by $\mathfrak{x}_k^l$. Therefore, by determining a certain constellation hierarchy, *i.e.*, under the condition of fixed P and fixed N_p, $\frac{1}{OT_{\text{tot}}}\sum_{o\in\mathcal{O}}\sum_{t=1}^{T_{\text{tot}}} F(N_P,P,h,i,\Omega,M_A)$ in eq. (24) can be simplified as $\frac{1}{OT_{\text{tot}}}\sum_{o\in\mathcal{O}}\sum_{t=1}^{T_{\text{tot}}} F_k^l(h,i,\Omega,M_A)$. Then combined with the footnote 11, $\mathfrak{x}_k^l$ can be shown below:

$$(\mathfrak{x}_k^l): \min -\overline{C} = -\frac{1}{OT_{\text{tot}}}\sum_{o\in\mathcal{O}}\sum_{t=1}^{T_{\text{tot}}} F_k^l(h,i,\Omega,M_A), \quad (29a)$$

$$\text{s.t.} \quad 250 \le h \le 500, \quad (29b)$$

$$0^\circ \le i \le 90^\circ, \quad (29c)$$

$$0^\circ \le \Omega, M_A \le 360^\circ, \quad (29d)$$

where $k \in \{1,2,...,N_{\text{tot}}\}$.

Algorithm 2: The "three-stage" algorithm to $\mathfrak{X}$

Input: N_{tot}, $\mathcal{O}$, $\mathfrak{M}$, $\mathfrak{T}_{\text{gmax}}$, $\mathbf{I}=[h,i,\Omega,M_A]$, constraints in eq. (28).

Initialization: Random initial population $\mathfrak{P}_0$, $n=1$;
while $n \le N_{\text{tot}}$ **do**
  Prime factorization of n, get L cases;
  for *each* $\mathfrak{x}$ *(L cycles in total)* **do**
    Solving based on Algorithm 1;
  Obtain $\overline{C}_{\max}^n$ and its corresponding optimal constellation hierarchy in the case of n, along with the corresponding optimal parameters $\mathbf{I}_{\text{opt}}^n$;
  $n = n+1$;

Output: $\overline{C}_{\max}^n$, $(N_P^n\text{-}P^n)_{\text{opt}}$, $\mathbf{I}_{\text{opt}}^n, \forall n \in \{1,...,N_{\text{tot}}\}$.

B. Stage 2: Solution to $\mathfrak{x}$: Elite Strategy Genetic Algorithm

Genetic algorithm belongs to an adaptive global optimal probabilistic search algorithm, which combines evolutionary theory and genetic doctrine, and uses computer technology to study and simulate the genetic and evolutionary process of organisms in their natural environment [44], [45].

The design variable of $\mathfrak{x}$, *i.e.*, a set of constellation parameters, is an individual or chromosome, as follows:

$$\mathbf{I} = [h,i,\Omega,M_A], \quad (30)$$

where h,i,Ω,M_A are the individual attributes of the individual, or the genes called chromosome.

Considering that the individuals involved in $\mathfrak{x}$ are multivariate constellation parameter individuals, an elite strategy is applied to replicate some of the contemporary optimal solutions directly into the next generation to prevent the optimal solutions generated in the evolutionary process from being destroyed by crossover and variation operations, thus significantly improving the computational speed of the algorithm. The elite strategic genetic algorithm (ESGA) can be simply expressed as follows:

$$ESGA = (\mathfrak{C},\mathfrak{F},\mathfrak{P}_0,\mathfrak{M},\mathfrak{N},\Phi,\Gamma,\Psi,\mathfrak{T}), \quad (31)$$

where $\mathfrak{C}$ is the coding method, $\mathfrak{F}$ is the individual fitness evaluation function, $\mathfrak{P}_0$ denotes the initial population, $\mathfrak{M}$ is the population size, $\mathfrak{N}$ is the elite value, Φ,Γ[12],Ψ denote the selection operator, the crossover operator, and the mutation operator, respectively. And $\mathfrak{T}$ is the termination condition of the genetic operation, which can be determined by the maximum number of genetic generations $\mathfrak{T}_{\text{gmax}}$. The pseudo code of the algorithm is shown in Algorithm 1, where $\Omega_{\text{opt}}^{\text{seed}}$ and $M_{A_{\text{opt}}}^{\text{seed}}$ denote the optimal Ω and the optimal M_A of the seed satellite, respectively.

Fig. 7 is a simplified flow illustration of ESGA.

1) Genetic Coding: Considering that the optimization problem $\mathfrak{x}$ is a multi-dimensional, high-precision required continuous function optimization problem, and the simulation software uses high-precision double-precision floating-point

[12]In this article, the symbol Γ is also used to denote the crossover fraction in the crossover operation.

representation for real number encoding, the *DoubleVector* encoding method is applied in this article. The encoding process can be expressed as follows:

$$[h, i, \Omega, M_A] \xrightarrow{\mathfrak{C}} [\mathbf{I}_1, \mathbf{I}_2, \mathbf{I}_3, \mathbf{I}_4]. \tag{32}$$

The specific coding follows the formula shown below:

$$\mathbf{I}_j = roundn\left(\frac{\mathbf{I}(j) - U(j)_{\text{low}}}{U(j)_{\text{upp}} - U(j)_{\text{low}}}, -\xi\right), j = 1, ..., 4, \xi \in \mathbb{Z}^+, \tag{33}$$

where $\mathbf{I}(j)$ is the truth value of the j^{th} variable, $\mathbf{I}_j$ and $[U(j)_{\text{low}}, U(j)_{\text{upp}}]$ are its coded values and the range of values taken. The coding precision ξ in the rounding function $round(\cdot)$ indicates the number of decimal places retained.

The corresponding decoding is shown as follows:

$$\mathbf{I}(j) = \mathbf{I}_j \cdot [U(j)_{\text{upp}} - U(j)_{\text{low}}] + U(j)_{\text{low}}, j = 1, ..., 4. \tag{34}$$

2) Individual Fitness: The function that measures the fitness of an individual is called the fitness function $\mathfrak{F}(\mathbf{I})$ and is generally converted from the target function $f_{\text{obj}}(\mathbf{I})$ or the penalty function $\phi(\mathbf{I}, r_j)$. A common conversion relation is shown below.

For the maximization problem, *i.e.*, $\max f_{\text{obj}}(\mathbf{I})$, the fitness function can be given by the following equation:

$$\mathfrak{F}(\mathbf{I}) = \begin{cases} f_{\text{obj}}(\mathbf{I}) + C_{\min}, f_{\text{obj}}(\mathbf{I}) + C_{\min} > 0 \\ 0, f_{\text{obj}}(\mathbf{I}) + C_{\min} \leq 0 \end{cases}, \tag{35}$$

where $C_{\min}$ is a suitably small positive number.

For the minimization problem, *i.e.*, $\min f_{\text{obj}}(\mathbf{I})$, the fitness function can then be given by

$$\mathfrak{F}(\mathbf{I}) = \begin{cases} C_{\max} - f_{\text{obj}}(\mathbf{I}), f_{\text{obj}}(\mathbf{I}) < C_{\max} \\ 0, f_{\text{obj}}(\mathbf{I}) \geq C_{\max} \end{cases}, \tag{36}$$

where $C_{\max}$ is a larger positive number.

3) Genetic Operations: Evolution is carried out with a population of population size $\mathfrak{M}$ as the main body, and the i^{th} generation population is denoted as $\mathfrak{P}_i$. Repeated selection, crossover and mutation of the population result in continuous overall optimization, obtaining optimal individuals.

• Selection operation Φ: The probability of individual q being selected in heredity is given by

$$Pr_{qs} = \mathfrak{F}_q / \sum_{q=1}^{\mathfrak{M}} \mathfrak{F}_q, \forall q = 1, ..., \mathfrak{M}, \tag{37}$$

where Pr_{qs} satisfies the probability sum of 1, *i.e.*,

$$\sum_{q=1}^{\mathfrak{M}} Pr_{qs} = 1. \tag{38}$$

A roulette wheel selection method was then used. A random number from 0 to 1 is generated randomly, determining which individuals are selected and how many times they are inherited. It should be emphasized that the introduction of the elitist strategy will directly replicate some of the optimal individuals of the contemporary generation to the next generation, but these optimal individuals will still need to participate in the roulette wheel selection subsequently.

TABLE I
MAIN PARAMETERS FOR SIMULATION

Parameter	Value
Minimum elevation angle $\theta_{\min}$	10°
Earth's Radius R_e	6378.14km
Earth's rotation period T_e	86164s *(24h 56m 4s)*
Population size $\mathfrak{M}$	64
Elite individual size $\mathfrak{N}$	3
Coding precision ξ	4
Crossover fraction Γ	0.8
Mutation operator Ψ	*Adaptive feasible*
Maximum generation $\mathfrak{T}_{\text{gmax}}$	100
Start time	1 May 2022 00:00:00.0
End time	1 May 2022 23:56:04.0
Time step	60s
Orbit prediction model	Twobody
Coordinate system	J2000

• Crossover operation Γ: consider the crossover-arithmetic method, following the below equation:

$$\mathbf{I}_{ab} = w_1 \mathbf{I}_a + w_2 \mathbf{I}_b, w_1 + w_2 = 1, \tag{39}$$

where the weights w_1 and w_2 can be adaptively adjusted according to the selection probability Pr_s. The progeny produced by this method is the weighted arithmetic mean between individual a and individual b, and it is easy to know that the progeny are always in the feasible domain.

• Mutation operation Ψ: Consider a random, bounded and linearly constrained direction and step size, which is adaptive compared to the last successful or unsuccessful generation.

C. Stage 3: Polymerization

After solving multiple single-objective optimization problems $\mathfrak{x}$ using Algorithm 1, the optimal coverage and its corresponding constellation parameters under various constellation hierarchies can be aggregated to solve $\mathfrak{X}$. Considering that the objectives in the multi-objective optimization problem $\mathfrak{X}$ are mutually exclusive, a compromise between maximizing the average coverage and minimizing the constellation scale is ultimately required, which is also consistent with the practical construction. And the brief pseudo code that can solve $\mathfrak{X}$ is shown in Algorithm 2.

Additionally, as mentioned before, due to the complexity of the constellation design problem itself, and the fact that the solution in this paper combines the application of genetic algorithm and constellation system construction, a larger constellation scale can cause a larger cost in terms of solving time. However, in order to take into account the observation of the performance of larger constellation scales, we compromise and consider simulating from the "1×1" hierarchy to the "$N_P \times P$" hierarchy. Concretely, we individually obtain the optimal constellation parameters from "1×1" hierarchy to "$N_P \times P$" hierarchy by ESGA. The polymerization results, in addition to examining the impact of different constellation scales and different constellation hierarchies on the coverage performance, are capable of determining the minimum constellation scale $N_{\text{tot}}^{\overline{C}_{\text{target}},\min}$ that satisfies any given metric target $\overline{C}_{\text{target}}$, where $N_{\text{tot}}^{\overline{C}_{\text{target}},\min}$ should be those scale cases for

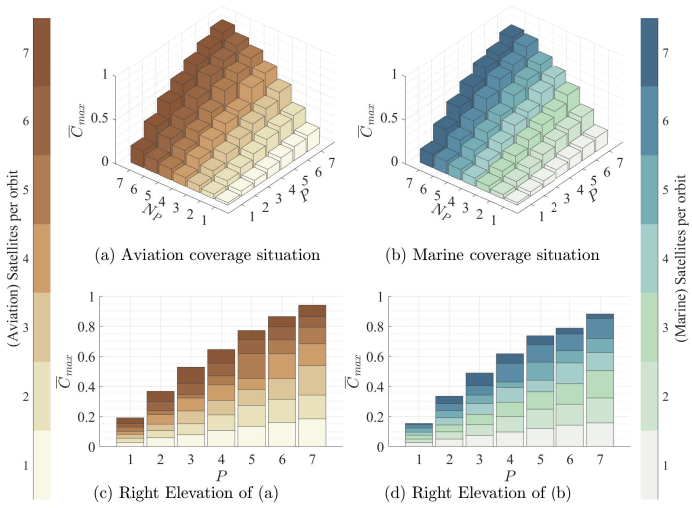

Fig. 8. Maximum average coverage rate $\overline{C}_{\max}$.

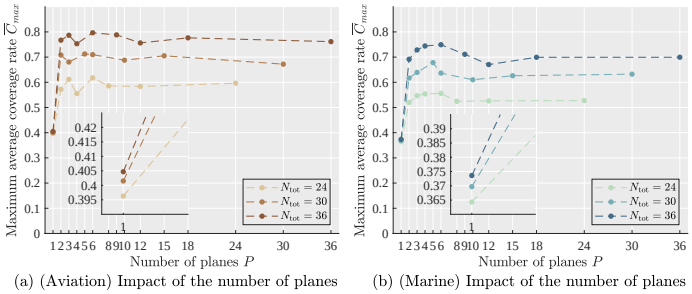

Fig. 9. Impact of the number of planes on performance with fixed N_{tot}.

which all factorization cases can be found. Then, by factorizing $N_{\text{tot}}^{\overline{C}_{\text{target}},\min}$ and comparing the constellation performance of different hierarchies, the optimal constellation hierarchy $(N_P\text{-}P)_{\text{opt}}$, which is also demanded by $\mathfrak{X}$, can be obtained by the way. A more detailed interpretation can be provided by the simulation analysis in Section V-B.

V. Simulation Result

In this section, we present and analyze the simulation results. Before that we need a brief explanation of the settings of the main parameters.

In the application of ESGA algorithm, the setting of $\mathfrak{M}$ should be no less than 50 in order to avoid the algorithm converging to the local optimal solution rapidly, but too large $\mathfrak{M}$ will also bring a sharp increase in spatial and temporal resources. Due to the limited arithmetic and time resources, we consider a population scale $\mathfrak{M}$ of 64, and the proportion of elite individuals $\mathfrak{N}$ is controlled to 5%, *i.e.*, $0.05\mathfrak{M}$. Other parameters related to the algorithm are set mainly to serve better performance metrics and accuracy.

The main parameter values of the algorithm and the satellite simulation system are shown in Table I.

A. Maximum Average Coverage Rate

From Fig. 8 we can observe that the maximum average coverage can be improved by increasing N_P by fixing P or increasing P by fixing N_P, which is in complete accordance with the actual situation. And for larger constellation scales with more severe coverage overlap in a single plane, increasing the number of planes can significantly improve coverage performance, as shown in Fig. 9.

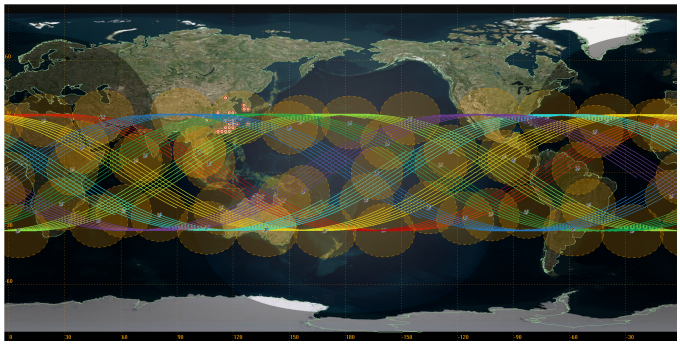

Fig. 10. Aviation part of the optimal constellation (7×7).

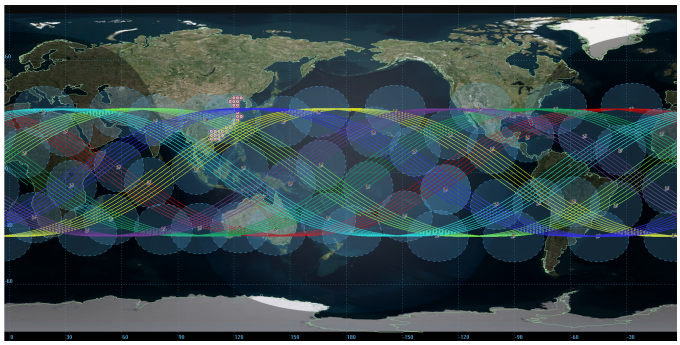

Fig. 11. Marine part of the optimal constellation (7×7).

The optimal constellation parameters of the VLEO satellite constellations from "1×1" to "7×7" layer configuration and their corresponding coverage rate are shown in Table II. And the actual satellite scenarios corresponding to the constellation parameters of "7×7" layer configuration are shown in Fig. 10 and Fig. 11, from which it can be seen that the optimal constellations have satisfactory coverage of the communication business requirements in respective BOP region. And the maximum average coverage of ACT part has reached 94.11%, while MCT part has reached nearly 90%.

Taking into account the actual construction costs and the realistic situation of communication service needs, and given the altitude of the VLEO satellite, a coverage of more than 90% can generally mean that we can use the optimal parameters in Table II as the actual parameters to deploy the VLEO satellite constellation for the target area.

B. Optimal Satellite Constellation Hierarchy

For further study, for any given average coverage in the target region, the corresponding optimal VLEO constellation, including satellite hierarchy and constellation parameters, can be obtained, Fig. 12 shows the optimal constellation hierarchy for ACT and MCT parts of the target region based on Table II, respectively.

TABLE II
($1 \times 1 - 7 \times 7$) OPTIMAL CONSTELLATION PARAMETERS AND ITS CORRESPONDING COVERAGE ("$(\mathbf{1 \times 1})$" $\Leftrightarrow$ "$\mathbf{Value}(\mathbf{1 \times 1})$")

Parameter	h_{opt}	i_{opt}	$\Omega_{\text{opt}}^{\text{seed}}$	$M_{A_{\text{opt}}}^{\text{seed}}$	$\overline{C}_{\max}$	**Parameter**	h_{opt}	i_{opt}	$\Omega_{\text{opt}}^{\text{seed}}$	$M_{A_{\text{opt}}}^{\text{seed}}$	$\overline{C}_{\max}$
$(\mathbf{1 \times 1})$	490.3767km	35.3004°	158.9110°	345.3449°	0.0265	$(\mathbf{1 \times 1})$	472.0679km	32.6526°	187.8737°	94.8596°	0.0258
$(\mathbf{1 \times 2})$	499.1552km	34.7733°	359.3316°	160.0362°	0.0545	$(\mathbf{1 \times 2})$	496.8668km	33.2926°	5.0113°	274.0323°	0.0493
$(\mathbf{1 \times 3})$	483.2586km	33.5153°	231.3484°	150.3225°	0.0798	$(\mathbf{1 \times 3})$	492.9503km	32.6438°	295.2230°	233.8803°	0.0750
$(\mathbf{1 \times 4})$	466.4712km	33.0274°	208.9508°	234.3661°	0.1003	$(\mathbf{1 \times 4})$	480.6147km	33.1118°	220.8371°	264.4800°	0.0947
$(\mathbf{1 \times 5})$	471.8322km	33.7196°	199.9691°	203.1372°	0.1287	$(\mathbf{1 \times 5})$	494.7723km	32.9568°	338.2819°	139.8201°	0.1224
$(\mathbf{1 \times 6})$	473.9101km	34.4592°	289.5776°	62.9678°	0.1530	$(\mathbf{1 \times 6})$	489.4851km	33.4655°	200.7225°	59.8121°	0.1466
$(\mathbf{1 \times 7})$	499.0883km	34.2965°	149.9342°	124.6807°	0.1906	$(\mathbf{1 \times 7})$	453.8087km	34.3390°	101.0617°	228.9029°	0.1531
$(\mathbf{2 \times 1})$	495.9636km	35.4911°	103.1086°	228.5867°	0.0582	$(\mathbf{2 \times 1})$	490.3640km	35.3621°	158.8561°	345.1552°	0.0493
$(\mathbf{2 \times 2})$	475.7595km	33.4551°	154.2067°	265.8482°	0.1050	$(\mathbf{2 \times 2})$	491.0422km	35.3307°	159.7829°	345.0059°	0.0968
$(\mathbf{2 \times 3})$	468.1447km	36.0721°	322.0243°	94.9198°	0.1481	$(\mathbf{2 \times 3})$	489.6697km	35.2379°	160.4462°	345.3281°	0.1430
$(\mathbf{2 \times 4})$	495.9804km	33.0875°	76.1696°	138.1198°	0.2115	$(\mathbf{2 \times 4})$	489.6267km	35.3004°	160.4110°	345.3449°	0.1902
$(\mathbf{2 \times 5})$	442.1341km	33.1002°	261.8085°	262.3373°	0.2395	$(\mathbf{2 \times 5})$	490.3767km	35.3004°	158.9110°	345.3449°	0.2382
$(\mathbf{2 \times 6})$	460.5164km	33.6777°	206.5371°	239.4197°	0.2995	$(\mathbf{2 \times 6})$	490.3767km	35.3004°	160.4110°	345.3449°	0.2842
$(\mathbf{2 \times 7})$	481.8171km	34.0934°	163.7447°	156.6536°	0.3676	$(\mathbf{2 \times 7})$	490.3767km	35.3004°	158.9110°	345.3449°	0.3347
$(\mathbf{3 \times 1})$	476.5009km	33.8821°	27.6177°	307.3797°	0.0784	$(\mathbf{3 \times 1})$	490.4686km	35.1818°	159.9747°	345.3084°	0.0729
$(\mathbf{3 \times 2})$	458.1344km	33.8001°	251.3051°	241.9330°	0.1509	$(\mathbf{3 \times 2})$	490.3767km	35.3004°	158.9110°	345.3449°	0.1447
$(\mathbf{3 \times 3})$	479.7200km	34.0150°	120.0162°	88.9287°	0.2361	$(\mathbf{3 \times 3})$	489.6267km	35.3004°	160.4110°	345.3449°	0.2135
$(\mathbf{3 \times 4})$	493.8070km	34.3661°	31.3871°	121.3930°	0.3220	$(\mathbf{3 \times 4})$	489.6267km	35.3004°	160.4110°	345.3449°	0.2857
$(\mathbf{3 \times 5})$	436.6606km	35.5382°	320.3785°	274.7304°	0.3460	$(\mathbf{3 \times 5})$	469.6820km	34.6213°	242.7803°	213.0882°	0.3422
$(\mathbf{3 \times 6})$	435.6109km	33.8594°	171.2320°	295.4418°	0.4202	$(\mathbf{3 \times 6})$	463.2823km	34.3403	269.4561°	171.3840°	0.4038
$(\mathbf{3 \times 7})$	472.2356km	32.5055°	249.2337°	175.8951°	0.5281	$(\mathbf{3 \times 7})$	482.3040km	34.5968°	164.4720°	334.9311°	0.4891
$(\mathbf{4 \times 1})$	467.9553km	33.6988°	204.5311°	137.7286°	0.1044	$(\mathbf{4 \times 1})$	490.3767km	35.3004°	158.9110°	345.3449°	0.0958
$(\mathbf{4 \times 2})$	485.6345km	33.0613°	281.7026°	164.7837°	0.2098	$(\mathbf{4 \times 2})$	496.9847km	33.0073°	107.0030°	223.6551°	0.2001
$(\mathbf{4 \times 3})$	470.5951km	35.1548°	85.2470°	255.8932°	0.3067	$(\mathbf{4 \times 3})$	494.7304km	33.2410°	101.6107°	228.1066°	0.2949
$(\mathbf{4 \times 4})$	481.7285km	31.6755°	263.3132°	146.0366°	0.4104	$(\mathbf{4 \times 4})$	494.1168km	32.8041°	98.5349°	216.6162°	0.3925
$(\mathbf{4 \times 5})$	447.2073km	32.5383°	96.6999°	8.1268°	0.4697	$(\mathbf{4 \times 5})$	460.7485km	35.4390°	206.6701°	283.2912°	0.4293
$(\mathbf{4 \times 6})$	433.6786km	31.8961°	188.9085°	37.0557°	0.5551	$(\mathbf{4 \times 6})$	498.1945km	33.4051°	105.4131°	224.3161°	0.5539
$(\mathbf{4 \times 7})$	433.8310km	32.5260°	97.8115°	198.9906°	0.6456	$(\mathbf{4 \times 7})$	480.9685km	31.6798°	149.5738°	218.4790°	0.6173
$(\mathbf{5 \times 1})$	490.3767km	35.3004°	158.9110°	345.3449°	0.1342	$(\mathbf{5 \times 1})$	476.3759km	33.3821°	28.0986°	307.8606°	0.1197
$(\mathbf{5 \times 2})$	499.3133km	34.2457°	99.5251°	225.5875°	0.2738	$(\mathbf{5 \times 2})$	499.3602km	33.6989°	99.1501°	225.4469°	0.2486
$(\mathbf{5 \times 3})$	471.9066km	32.0789°	172.7926°	87.0331°	0.3791	$(\mathbf{5 \times 3})$	499.3602km	33.6989°	99.1501°	225.4469°	0.3638
$(\mathbf{5 \times 4})$	424.5188km	31.9430°	192.1423°	50.0313°	0.4527	$(\mathbf{5 \times 4})$	454.3131km	32.2387°	179.5776°	195.7660°	0.4411
$(\mathbf{5 \times 5})$	476.8468km	35.3432°	263.2437°	251.9972°	0.6178	$(\mathbf{5 \times 5})$	476.6572km	33.6462°	160.6218°	147.5719°	0.5611
$(\mathbf{5 \times 6})$	492.3068km	34.1716°	169.9359°	320.0534°	0.7124	$(\mathbf{5 \times 6})$	499.5664km	34.7346°	195.8157°	150.4658°	0.6781
$(\mathbf{5 \times 7})$	439.1847km	33.2439°	232.5211°	169.6227°	0.7723	$(\mathbf{5 \times 7})$	481.3916km	34.4563°	163.4827°	333.8515°	0.7370
$(\mathbf{6 \times 1})$	481.4468km	34.6344°	174.1082°	106.5457°	0.1591	$(\mathbf{6 \times 1})$	488.7619km	35.2540°	162.1144°	337.9021°	0.1416
$(\mathbf{6 \times 2})$	497.1911km	35.6777°	112.2566°	286.0484°	0.3141	$(\mathbf{6 \times 2})$	477.1096km	33.1645°	24.4028°	310.3875°	0.2813
$(\mathbf{6 \times 3})$	465.9701km	34.8906°	286.7605°	115.0045°	0.4526	$(\mathbf{6 \times 3})$	477.4628km	33.4962°	33.7928°	305.8302°	0.4180
$(\mathbf{6 \times 4})$	478.0509km	32.4602°	178.7247°	61.6480°	0.6177	$(\mathbf{6 \times 4})$	487.3475km	35.4684°	53.6605°	21.7304°	0.556
$(\mathbf{6 \times 5})$	485.8320km	30.6724°	118.3862°	82.6413°	0.7098	$(\mathbf{6 \times 5})$	475.9764km	34.9318°	152.3235°	144.4319°	0.6365
$(\mathbf{6 \times 6})$	484.5602km	33.2038°	258.6961°	111.5804°	0.7965	$(\mathbf{6 \times 6})$	490.3727km	34.1647°	204.0337°	61.5224°	0.7492
$(\mathbf{6 \times 7})$	481.8553km	34.5522°	164.7541°	334.2705°	0.8655	$(\mathbf{6 \times 7})$	476.9857km	31.3689°	203.8733°	224.2263°	0.7881
$(\mathbf{7 \times 1})$	478.5763km	35.2221°	61.3587°	218.5676°	0.1835	$(\mathbf{7 \times 1})$	453.6793km	31.6874°	302.6402°	141.4281°	0.1567
$(\mathbf{7 \times 2})$	452.5691km	33.7551°	213.4557°	124.5597°	0.3417	$(\mathbf{7 \times 2})$	478.2200km	31.5980°	193.5021°	230.2329°	0.3229
$(\mathbf{7 \times 3})$	473.4560km	34.0280°	83.2930°	201.0901°	0.5378	$(\mathbf{7 \times 3})$	499.3602km	33.6989°	99.1501°	225.4469°	0.5047
$(\mathbf{7 \times 4})$	465.9083km	35.8659°	156.1300°	141.2162°	0.6840	$(\mathbf{7 \times 4})$	480.3515km	35.4463°	101.2227°	116.1264°	0.6256
$(\mathbf{7 \times 5})$	480.7570km	33.8009°	240.7562°	158.1593°	0.7948	$(\mathbf{7 \times 5})$	460.8291km	32.0099°	190.4914°	86.7499°	0.7195
$(\mathbf{7 \times 6})$	470.4727km	34.1455°	112.1273°	299.6051°	0.8651	$(\mathbf{7 \times 6})$	481.6179km	32.1408°	157.2281°	331.9862°	0.8521
$(\mathbf{7 \times 7})$	485.6304km	30.9944°	159.1224°	158.7314°	0.9411	$(\mathbf{7 \times 7})$	455.6770km	33.8998°	105.4312°	343.7436°	0.8822

The obvious conclusion from Fig. 12 is that the average coverage of the constellation increases with the expansion of N_{tot}, but as N_{tot} continues to grow, the improvement effect of its coverage performance tends to decrease gradually, showing a slowing down of the curve. Taking MCT part as an example, the average coverage performance index has almost no improvement after N_{tot} is enhanced from 42 to 49. Therefore, based on the cost of constellation scale, we can set the average coverage target at 90% to greatly reduce the construction cost of constellation. In practice, this can be used as a compromise inflection point to build a effective and cost-controllable satellite constellation.

It should be added that the number on the curve indicates P corresponding to the optimal hierarchy at that satellite scale, based on which the specific optimal hierarchy for that case can be obtained based on the value of N_{tot}. Therefore, combined Table II with Fig. 12, the minimum number of satellites and the optimal constellation configuration for a given satellite scale can be determined when the maximum coverage is desired. Also taking MCT part as an example, considering a coverage target of 14%, N_{tot} has four feasible layer construction schemes for 6, namely "1×6", "2×3", "3×2", and "6×1". The simulation results show that 6 satellites is the minimum constellation scale and "1×6" is the optimal layer configuration scheme with a maximum average coverage of 0.1466, and the values of the last three are 0.1430, 0.1447, 0.1416, respectively.

Therefore, according to this figure, we can make a trade-off between the constellation scale, *i.e.*, constellation construction cost, and the user coverage, then obtain the optimal constel-

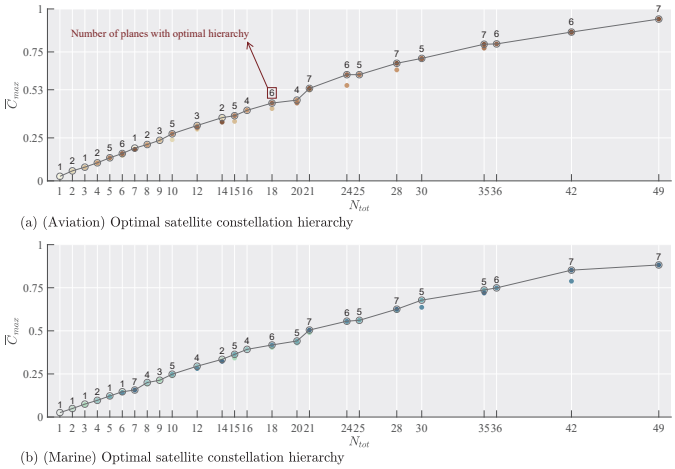

(a) (Aviation) Optimal satellite constellation hierarchy

(b) (Marine) Optimal satellite constellation hierarchy

Fig. 12. Constellation scale and optimal satellite constellation hierarchy.

lation hierarchy under the specific constellation scale.

C. Optimal Orbital Altitude and Incline

To evaluate the distribution characteristics of the optimal constellation parameters for various satellite scales, Fig. 13 and Fig. 14 give the distribution plots of h_{opt} and i_{opt}.

From Fig. 13, we can see that the spatial distribution of h_{opt} tends to 500 km regardless of the business and the constellation hierarchy. Theoretically, for the consideration and deployment of h without incorporating operational constraints, such as time-sensitive constraint and throughput constraint, the choice of large h can directly lead to an effective improvement in coverage, increase the link duration visibility time of the satellite, and further improve the average coverage of the target area. Considering the fact that there is no penalty constraint for large h in $\mathfrak{X}$, and based on the fact that the larger h, the larger the coverage, and the coverage is directly related to the objective function, the choice of large h is preferred in order to strive for a larger average coverage.

And as we can see in Fig. 14, the spatial distribution of i_{opt} tends to be in the latitude range of the target region. This can also be observed from the "7×7" optimal constellations in Fig. 10 and Fig. 11. In general, low inclination satellites are closer to the equator, have wider coverage, and provide better coverage of lower latitudes. Too large an orbital inclination results in greater equatorial deviation and narrower coverage. Given the fact that the orbital inclination of the optimal constellation is directly related to the distribution of BOPs, and considering that the target region is a low latitude region, a low orbital inclination, or angle selection near the latitude range of the operational distribution of the target region, is a very reasonable deployment decision.

Taken together, the orbital altitude and orbital inclination of the optimal constellation in the context of this optimization problem are characterized by large altitude with large coverage as well as low inclination with low latitude. This has a certain reference value and guidance for the design of actual area-oriented VLEO satellite constellations.

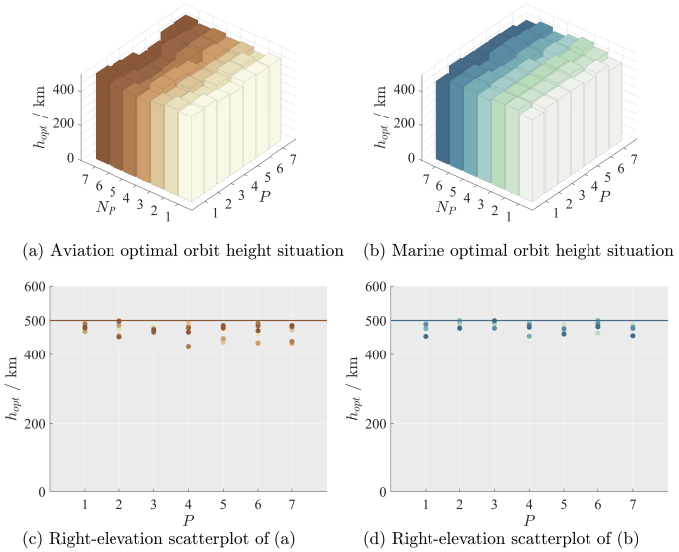

(a) Aviation optimal orbit height situation (b) Marine optimal orbit height situation

(c) Right-elevation scatterplot of (a) (d) Right-elevation scatterplot of (b)

Fig. 13. Optimal constellation orbit altitude.

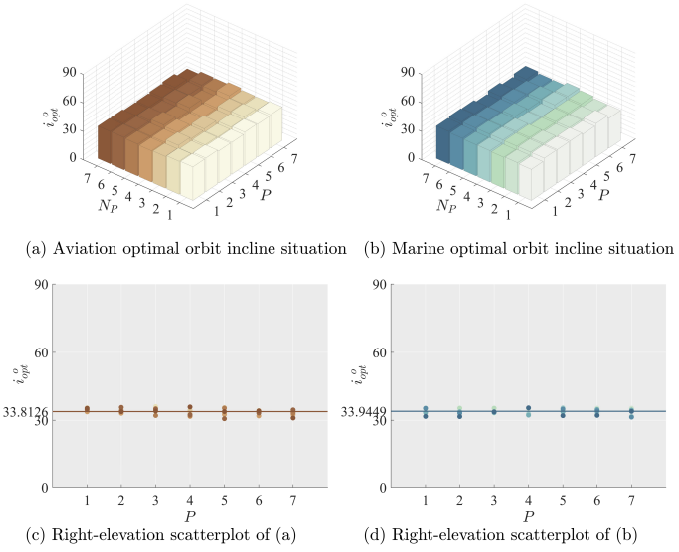

(a) Aviation optimal orbit incline situation (b) Marine optimal orbit incline situation

(c) Right-elevation scatterplot of (a) (d) Right-elevation scatterplot of (b)

Fig. 14. Optimal constellation orbit incline.

D. Spatial Distribution of BOPs

To evaluate the impact of business type, Fig. 15 compares the coverage situation for ACT and MCT for the same constellation scale. For the BOP distribution of ACT, the latitude and longitude range can be determined from Fig. 5 as [104°E-128°E, 22°N-40°N], while the BOP distribution of MCT can be determined from Fig. 6 as [108°E-124°E, 18°N-40°N]. In comparison, the former has a larger longitudinal range, while the latter has a larger latitudinal range.

From Fig. 15, we can find that the coverage performance of the aviation-oriented part, *i.e.*, the maximum average coverage rate, is always better than that of the marine part for the same constellation scale. Combined with the previous consideration of the optimal orbital inclination, we can know that the orbital inclination is always around 34° due to the fact that the optimal inclination is directly related to the spatial latitude of the operational distribution, limited by the low latitude of the

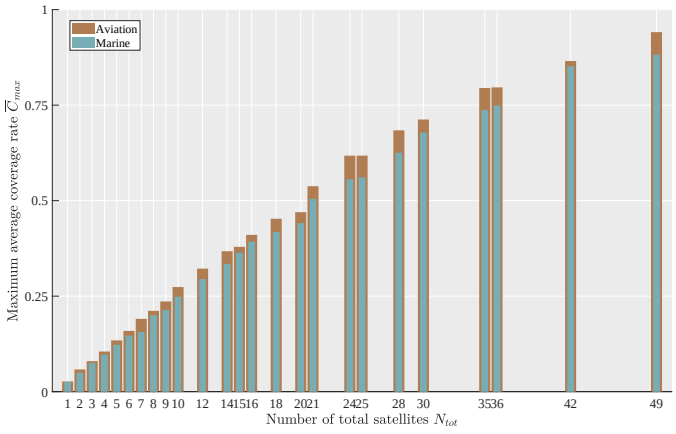

Fig. 15. Comparison of different spatial distributions.

target area. With such orbital inclination, combined with the constellation trajectory in Fig. 10 and Fig. 11 we can learn that the satellite constellation has a better coverage performance for the target area in the longitude range. In other words, our optimal VLEO satellite constellation is more inclined to cover longitudinally extended business, and the coverage performance at large longitude range should be better than that at large latitude range.

VI. Conclusion and Future Work

In this article, we have designed the constellation of VLEO satellites for AUs and MUs in the Chinese region. To ensure the authenticity and freshness of our work, we have generated the heat maps and BOP models for regional ACT and MCT using grid point method with the real ADS-B and AIS data we collected. Then we have derived the average coverage formula and proposed an IMOCM optimization problem to achieve the maximum average coverage with minimum satellites. And a "three-stage" solution, which combined the "divide-and-conquer" methodology and ESGA, has been proposed. For the implicit function value obtainment, we have built the corresponding constellation simulation system for joint simulation. The results have shown that for any given coverage requirement, the corresponding optimal VLEO constellation can be obtained and it is favor the deployment scheme of large orbital altitude, low orbital inclination and longitudinal distribution business, while the coverage performance will be reduced when facing the latitudinal distribution business.

Due to the highly migratory quality of our work, this article will be a reference for more countries and institutions to participate in the design and deployment of VLEO constellation in the future, especially for cost-efficient regional coverage. Besides, it also provide some new insights for the non-terrestrial network design.

With the future, under the framework of the whole constellation design process in this work, in order to provide more meaningful references for the actual constellation design and deployment work, we will consider investigating the application and performance comparison of different intellectual algorithms and the comparison of the results, which can optimize the framework and support a more efficient constellation design. In addition, optimal constellation analysis from the perspective of service distribution densities (*e.g.*, decentralized sparse and centralized dense) will be considered to be further researched. Furthermore, we will consider studying the design of integrated constellations with more objectives involved, such as integrated constellations based on the context of integration of communication and navigation.

References

[1] J. Navarro-Ortiz, P. Romero-Diaz, S. Sendra, P. Ameigeiras, J. J. Ramos-Munoz, and J. M. Lopez-Soler, "A survey on 5G usage scenarios and traffic models," *IEEE Communications Surveys & Tutorials*, vol. 22, no. 2, pp. 905–929, 2020.

[2] T. Chailungka, P. Horma, C. Juthamanee, W. Vongsantivanich, and S. Chaimatanan, "Geo-Information platform for visualisation, analysis and optimization for aviation," in *2017 10th International Conference on Ubi-media Computing and Workshops (Ubi-Media)*. IEEE, 2017, pp. 1–4.

[3] G. Soldi, D. Gaglione, N. Forti, A. Di Simone, F. C. Daffinà, G. Bottini, D. Quattrociocchi, L. M. Millefiori, P. Braca, S. Carniel *et al.*, "Space-based global maritime surveillance. Part I: Satellite technologies," *IEEE Aerospace and Electronic Systems Magazine*, vol. 36, no. 9, pp. 8–28, 2021.

[4] H. Guo, J. Li, J. Liu, N. Tian, and N. Kato, "A survey on space-air-ground-sea integrated network security in 6G," *IEEE Communications Surveys & Tutorials*, vol. 24, no. 1, pp. 53–87, 2021.

[5] H. Cui, J. Zhang, Y. Geng, Z. Xiao, T. Sun, N. Zhang, J. Liu, Q. Wu, and X. Cao, "Space-air-ground integrated network (SAGIN) for 6G: Requirements, architecture and challenges," *China Communications*, vol. 19, no. 2, pp. 90–108, 2022.

[6] Q. Chen, W. Meng, S. Li, C. Li, and H.-H. Chen, "Civil aircrafts augmented space–air–ground-integrated vehicular networks: Motivation, breakthrough, and challenges," *IEEE Internet of Things Journal*, vol. 9, no. 8, pp. 5670–5683, 2021.

[7] Q. Cai, S. Alam, and V. Duong, "On robustness paradox in air traffic networks," *IEEE Transactions on Network Science and Engineering*, vol. 7, no. 4, pp. 3087–3099, 2020.

[8] A. Baltaci, E. Dinc, M. Ozger, A. Alabbasi, C. Cavdar, and D. Schupke, "A survey of wireless networks for future aerial communications (facom)," *IEEE Communications Surveys & Tutorials*, vol. 23, no. 4, pp. 2833–2884, 2021.

[9] K. Sampigethaya, R. Poovendran, S. Shetty, T. Davis, and C. Royalty, "Future e-enabled aircraft communications and security: The next 20 years and beyond," *Proceedings of the IEEE*, vol. 99, no. 11, pp. 2040–2055, 2011.

[10] A. Alessandrini, F. Mazzarella, and M. Vespe, "Estimated time of arrival using historical vessel tracking data," *IEEE Transactions on Intelligent Transportation Systems*, vol. 20, no. 1, pp. 7–15, 2018.

[11] M. Zhao, X. Yao, J. Sun, S. Zhang, and J. Bai, "Gis-based simulation methodology for evaluating ship encounters probability to improve maritime traffic safety," *IEEE Transactions on Intelligent Transportation Systems*, vol. 20, no. 1, pp. 323–337, 2018.

[12] S. Yu, X. Gong, Q. Shi, X. Wang, and X. Chen, "EC-SAGINs: Edge-computing-enhanced space–air–ground-integrated networks for internet of vehicles," *IEEE Internet of Things Journal*, vol. 9, no. 8, pp. 5742–5754, 2021.

[13] C. Jiang and X. Zhu, "Reinforcement learning based capacity management in multi-layer satellite networks," *IEEE Transactions on Wireless Communications*, vol. 19, no. 7, pp. 4685–4699, 2020.

[14] Z. Zhang, Y. Li, C. Huang, Q. Guo, L. Liu, C. Yuen, and Y. L. Guan, "User activity detection and channel estimation for grant-free random access in LEO satellite-enabled Internet of Things," *IEEE Internet of Things journal*, vol. 7, no. 9, pp. 8811–8825, 2020.

[15] N. U. Hassan, C. Huang, C. Yuen, A. Ahmad, and Y. Zhang, "Dense small satellite networks for modern terrestrial communication systems: Benefits, infrastructure, and technologies," *IEEE Wireless Communications*, vol. 27, no. 5, pp. 96–103, 2020.

[16] X. Lv, S. Wu, A. Li, J. Jiao, N. Zhang, and Q. Zhang, "A Weighted Graph-Based Handover Strategy for Aeronautical Traffic in LEO SatCom Networks," *IEEE Networking Letters*, vol. 4, no. 3, pp. 132–136, 2022.

[17] Z. Jia, M. Sheng, J. Li, and Z. Han, "Toward Data Collection and Transmission in 6G Space–Air–Ground Integrated Networks: Cooperative HAP and LEO Satellite Schemes," *IEEE Internet of Things Journal*, vol. 9, no. 13, pp. 10 516–10 528, 2021.
[18] Y. Cai, S. Wu, J. Luo, J. Jiao, N. Zhang, and Q. Zhang, "Age-oriented access control in GEO/LEO heterogeneous network for marine IoRT: A deep reinforcement learning approach," *IEEE Internet of Things Journal*, vol. 9, no. 24, pp. 24 919–24 932, 2022.
[19] P. Gu, R. Li, C. Hua, and R. Tafazolli, "Dynamic cooperative spectrum sharing in a multi-beam LEO-GEO co-existing satellite system," *IEEE Transactions on Wireless Communications*, vol. 21, no. 2, pp. 1170–1182, 2021.
[20] G. Cui, P. Duan, L. Xu, and W. Wang, "Latency Optimization for Hybrid GEO-LEO Satellite Assisted IoT Networks," *IEEE Internet of Things Journal*, 2022.
[21] B. Al Homssi, A. Al-Hourani, K. Wang, P. Conder, S. Kandeepan, J. Choi, B. Allen, and B. Moores, "Next generation mega satellite networks for access equality: Opportunities, challenges, and performance," *IEEE Communications Magazine*, vol. 60, no. 4, pp. 18–24, 2022.
[22] S. Liu, Z. Gao, Y. Wu, D. W. K. Ng, X. Gao, K.-K. Wong, S. Chatzinotas, and B. Ottersten, "LEO satellite constellations for 5G and beyond: How will they reshape vertical domains?" *IEEE Communications Magazine*, vol. 59, no. 7, pp. 30–36, 2021.
[23] M. Y. Abdelsadek, A. U. Chaudhry, T. Darwish, E. Erdogan, G. Karabulut-Kurt, P. G. Madoery, O. B. Yahia, and H. Yanikomeroglu, "Future space networks: Toward the next giant leap for humankind," *IEEE Transactions on Communications*, vol. 71, no. 2, pp. 949–1007, 2022.
[24] L. Cheng, S. Liu, L. Liu, H. Hu, J. Chen, X. Mneg, and P. Ding, "Study on Gateway Station Deployment for Large Scale LEO Satellite Constellation Networks," in *2022 IEEE International Conference on Trust, Security and Privacy in Computing and Communications (TrustCom)*. IEEE, 2022, pp. 1540–1544.
[25] Y. Si, E. Zhang, W. Zhang, H. Ma, and T. Wu, "A Survey on the Development of Low-Orbit Mega-Constellation and Its TT&C Methods," in *2022 5th International Conference on Information Communication and Signal Processing (ICICSP)*. IEEE, 2022, pp. 324–332.
[26] G. M. Capez, M. A. Caceres, C. Bridges, S. Frey, R. Armellin, R. Garello, and P. Bargellini, "Characterisation of Mega-Constellation Links for LEO Missions with Applications to EO and ISS Use Cases," *IEEE Access*, 2023.
[27] R. Deng, B. Di, S. Chen, S. Sun, and L. Song, "Ultra-dense LEO satellite offloading for terrestrial networks: How much to pay the satellite operator?" *IEEE Transactions on Wireless Communications*, vol. 19, no. 10, pp. 6240–6254, 2020.
[28] R. Deng, B. Di, H. Zhang, L. Kuang, and L. Song, "Ultra-dense LEO satellite constellations: How many LEO satellites do we need?" *IEEE Transactions on Wireless Communications*, vol. 20, no. 8, pp. 4843–4857, 2021.
[29] C.-J. Wang, "Structural properties of a low earth orbit satellite constellation-the walker delta network," in *Proceedings of MILCOM'93-IEEE Military Communications Conference*, vol. 3. IEEE, 1993, pp. 968–972.
[30] D. C. Beste, "Design of satellite constellations for optimal continuous coverage," *IEEE Transactions on Aerospace and Electronic Systems*, no. 3, pp. 466–473, 1978.
[31] D. Mortari and M. P. Wilkins, "Flower constellation set theory. Part I: Compatibility and phasing," *IEEE Transactions on Aerospace and Electronic Systems*, vol. 44, no. 3, pp. 953–962, 2008.
[32] M. P. Wilkins and D. Mortari, "Flower constellation set theory part II: secondary paths and equivalency," *IEEE Transactions on Aerospace and Electronic Systems*, vol. 44, no. 3, pp. 964–976, 2008.
[33] D. Mortari, M. De Sanctis, and M. Lucente, "Design of flower constellations for telecommunication services," *Proceedings of the IEEE*, vol. 99, no. 11, pp. 2008–2019, 2011.
[34] B. Chen, Z. Li, and X. Yang, "Regional coverage scheme based on leo microsatellite formation," in *2012 IEEE Globecom Workshops*. IEEE, 2012, pp. 13–18.
[35] P. Wang, B. Di, and L. Song, "Multi-layer LEO satellite constellation design for seamless global coverage," in *2021 IEEE Global Communications Conference (GLOBECOM)*. IEEE, 2021, pp. 01–06.
[36] Y. Kim, Y. Song, and S. H. Lim, "Hierarchical maritime radio networks for internet of maritime things," *IEEE Access*, vol. 7, pp. 54 218–54 227, 2019.
[37] S. M. Dakka, "VLEO Satellites: A New Earth Observation Space Systems Commercial and Business Model," 2018.
[38] S. K. Sharma, S. Chatzinotas, and P.-D. Arapoglou, *Satellite communications in the 5G era*. Institution of Engineering and Technology, 2018.
[39] Y. Su, Y. Liu, Y. Zhou, J. Yuan, H. Cao, and J. Shi, "Broadband LEO satellite communications: Architectures and key technologies," *IEEE Wireless Communications*, vol. 26, no. 2, pp. 55–61, 2019.
[40] Z. Song, G. Dai, M. Wang, and X. Chen, "A novel grid point approach for efficiently solving the constellation-to-ground regional coverage problem," *IEEE Access*, vol. 6, pp. 44 445–44 458, 2018.
[41] C. Dai, G. Zheng, and Q. Chen, "Satellite constellation design with multi-objective genetic algorithm for regional terrestrial satellite network," *China Communications*, vol. 15, no. 8, pp. 1–10, 2018.
[42] I. Meziane-Tani, G. Métris, G. Lion, A. Deschamps, F. T. Bendimerad, and M. Bekhti, "Optimization of small satellite constellation design for continuous mutual regional coverage with multi-objective genetic algorithm," *International Journal of Computational Intelligence Systems*, vol. 9, no. 4, pp. 627–637, 2016.
[43] T. Savitri, Y. Kim, S. Jo, and H. Bang, "Satellite constellation orbit design optimization with combined genetic algorithm and semianalytical approach," *International Journal of Aerospace Engineering*, vol. 2017, 2017.
[44] I. Jerin Leno, S. Saravana Sankar, M. Victor Raj, and S. Ponnambalam, "An elitist strategy genetic algorithm for integrated layout design," *The International Journal of Advanced Manufacturing Technology*, vol. 66, pp. 1573–1589, 2013.
[45] I. Jerin Leno, S. Saravana Sankar, and S. Ponnambalam, "An elitist strategy genetic algorithm using simulated annealing algorithm as local search for facility layout design," *The International Journal of Advanced Manufacturing Technology*, vol. 84, pp. 787–799, 2016.

Guoquan Chen (Graduate Student Member, IEEE) received the B.E. degree in electronic and information engineering from the Harbin Institute of Technology (Shenzhen) in 2022, where he is currently pursuing the M.S. degree with the Department of Electronic Engineering. His research interests include space communications, satellite constellation design, and wireless communications.

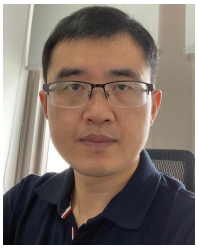

Shaohua Wu (Member, IEEE) received the Ph.D. degree in communication engineering from the Harbin Institute of Technology in 2009. From 2009 to 2011, he held a post-doctoral position at the Department of Electronics and Information Engineering, Shenzhen Graduate School, Harbin Institute of Technology, where he has been with since 2012. From 2014 to 2015, he was a Visiting Researcher with BBCR, University of Waterloo, Canada. He is currently a Full Professor with the Harbin Institute of Technology (Shenzhen), China. He is also a Professor with the Peng Cheng Laboratory, Shenzhen, China. His research interests include satellite and space communications, advanced channel coding techniques, space-air-ground-sea integrated networks, and B5G/6G wireless transmission technologies. He has authored or coauthored over 100 papers in these fields and holds over 40 Chinese patents.

Yajing Deng received the B.S. degree in communication engineering from Harbin Institute of Technology, China, in 2018, the M.S. degree in information and communication engineering from Harbin Institute of Technology (Shenzhen), China, in 2021. She is currently pursuing the Ph.D. degree in information and communication engineering with Harbin Institute of Technology (Shenzhen), Shenzhen, China. Her research interests include space communications, advanced channel coding techniques, real-time systems and wireless communications.

Jian Jiao (Member, IEEE) received the M.S. and Ph.D. degrees in communication engineering from the Harbin Institute of Technology (HIT), Harbin, China, in 2007 and 2011, respectively. From 2011 to 2015, he was a Post-Doctoral Research Fellow at the Communication Engineering Research Centre, Shenzhen Graduate School, HIT, Shenzhen, China. From 2016 to 2017, he was a China Scholarship Council Visiting Scholar with the School of Electrical and Information Engineering, The University of Sydney, Sydney, Australia. Since 2015, he has been with the School of Electrical and Information Engineering, HIT, where he is currently an Associate Professor. His research interests include error control codes, satellite communications, and massive RA.

Qinyu Zhang (Senior Member, IEEE) received the bachelor's degree in communication engineering from the Harbin Institute of Technology (HIT), Harbin, China, in 1994, and the Ph.D. degree in biomedical and electrical engineering from the University of Tokushima, Tokushima, Japan, in 2003. From 1999 to 2003, he was an Assistant Professor with the University of Tokushima. From 2003 to 2005, he was an Associate Professor with the Shenzhen Graduate School, HIT, and the Founding Director at the Communication Engineering Research Center, School of Electronic and Information Engineering (EIE). Since 2005, he has been a Full Professor and the Dean of the EIE School, HIT. His research interests include aerospace communications and networks, wireless communications and networks, cognitive radios, signal processing, and biomedical engineering. He has been a TPC Member of the Infocom, IEEE ICC, IEEE Globecom, IEEE Wireless Communications and Networking Conference, and other flagship conferences in communications. He was an Associate Chair of Finance of the International Conference on Materials and Manufacturing Technologies 2012, the TPC Co-Chair of the IEEE/CIC ICCC 2015, and the Symposium Co-Chair of the CHINACOM 2011 and the IEEE Vehicular Technology Conference 2016 (Spring). He was the Founding Chair of the IEEE Communications Society Shenzhen Chapter. He is on the Editorial Board of some academic journals, such as *Journal of Communication*, *KSII Transactions on Internet and Information Systems*, and *Science China Information Sciences*.